GeoEye-1: Analysis of Radiometric and Geometric Capability

Mattia Crespi[1], Gabriele Colosimo[1], Laura De Vendictis[2], Francesca Fratarcangeli[1], and Francesca Pieralice[1]

[1] Geodesy and Geomatic Area, University of Rome La Sapienza, Via Eudossiana 18, 00184 Rome, Italy
{mattia.crespi,gabriele.colosimo,francesca.fratarcangeli, francesca.pieralice}@uniroma1.it
http://w3.uniroma1.it/geodgeom/

[2] e-Geos S.p.A. - via Cannizzaro 71, 00156 Rome, Italy
guest517.devendictis@e-geos.it

Abstract. The Geoeye-1 satellite, launched in September 2008, is able to acquire imagery in panchromatic mode, with a spatial resolution of 0.41 m at nadir, offering the most powerful way to obtain detailed imagery actually commercially available.

The aim of the work is to evaluate the quality of the GeoEye-1 products through radiometric and geometric analysis; the area test is the city of Rome.

Radiometric quality of the image has been evaluated estimating the level of noise and the characteristic of the Modulation Transfer Function - MTF, that gives an index about the image sharpness.

The second part of the research is focused on the evaluation of the geometric capability of Geoeye-1 satellite. The image has been oriented using two different methods: the rigorous model and the Rational Polynomial Function (RPFs) model with the Rational Polynomial Coefficients (RPCs). The results were analysed in order to compare the orientation quality obtained from different model and different software, in terms of accuracy achievable from the image.

Keywords: HRSI, image orientation, radiometric quality.

1 Introduction

The Geoeye-1 satellite, launched in September 2008, is able to acquire imagery in panchromatic mode, with a spatial resolution of 0.41 m at nadir, and in multispectral mode, with a spatial resolution of 2.0 m at nadir, offering the most powerful way to obtain detailed imagery actually commercially available.

The aim of the work is to evaluate the quality of the GeoEye-1 products through radiometric and geometric analysis; the area test is the city of Rome.

The panchromatic analysed image was acquired on 21 September 2009, it has 0.5 m pixel size and belongs to the Geo product class. The Geo products are radiometrically corrected map oriented image, suitable for a wide range of uses.

K. Sithamparanathan et al. (Eds.): PSATS 2010, LNICST 43, pp. 354–369, 2010.

In addition to being suitable for visualization and monitoring applications, the Geo is shipped with the sensor camera model in Rational Polynomial Coefficients (RPCs) format. Geo images are projected onto an "inflated" ellipsoid, derived from the WGS84, choosing a certain ellipsoidal height. This kind of pre-processed images are usually mentioned as level 1B imagery.

Radiometric quality of the image has been evaluated estimating the level of noise and the characteristic of the Modulation Transfer Function - MTF, that gives an index about the image sharpness.

As regards the image noise, following the methods proposed from Baltsavias [1], the level of noise has been analysed by the standard deviation of the Digital Number of pixel selected in non-homogenous areas, so that a possible dependence between noise and radiometric intensity is evaluated.

The sharpness of the images has been analysed through the study of the Modulation Transfer Function; this function, in the spatial frequency domain for a chosen direction, represents the spatial resolution of the image. In order to estimate the MTF, an "edge method", proposed by Choi [2] and revised by De Vendictis [5], has been applied, using natural targets detected on the image.

The second part of the research is focused on the evaluation of the geometric capability of Geoeye-1 satellite. Tests of image orientation, using commercial and scientific software, have been performed. The image has been oriented using two different methods: the rigorous model and the Rational Polynomial Function (RPFs) model with the Rational Polynomial Coefficients (RPCs).

The results were analysed in order to compare the orientation quality obtained from different models in terms of accuracy achievable from the image. Two different software have been used: the commercial software PCI Geomatica 10.2 in which is included the rigorous model developed by Toutin, and the scientific software SISAR developed by the Geodesy and Geomatic Area of the University of Rome "La Sapienza".

The rigorous model implemented in SISAR is based on well know collinearity equations, with the reconstruction of the orbital segment during the image acquisition, the satellite position and attitude parameters.

Besides in the SISAR software it is possible to use RPCs and refine the image orientation on the basis of a set of GCPs. A possible refinement of the model, allowing for bias compensation, is accomplished in a quite common way with the introduction of a simple first order polynomial in the RPF, whose parameters are estimated.

2 Radiometric Quality Analysis

Within the chain from image sensing to the final value-added product, the imagery quality plays obviously a crucial role. Nowadays, most of the linear array sensors have the ability to provide more than 8-bit/pixel digital images; anyway we have still to consider some radiometric problems as the variations in the sensor view angle, the sun angle and shadowing, the image noise that can influence the image matching algorithms and the image unsharpness, due to CCD line jitter, kappa jitter and motion blur, and deficiencies of the lens system [11].

Image quality may be represented by several parameters as the radiometric resolution and its accuracy, represented by the noise level and the geometrical resolution and sharpness, described by the Modulation Transfer Function (MTF).

2.1 Noise Analysis

Here the noise level is evaluated through the standard deviation of the Digital Number (DN) in non-homogeneous areas according to the method proposed in Baltsavias et al. [1] and Zhang [11], that allow an analysis of the noise variation as a function of intensity. Usually the image noise is estimated using the standard deviation of the DN in homogeneous areas where one type surface's pixels should have the same DN; in any case homogeneous areas are not really representative of a standard acquisition and, moreover, the use of inhomogeneous areas allows an analysis of the noise variation as a function of intensity.

Nevertheless, if inhomogeneous areas are considered, it has to be taken in account on the entire image that the DN differences can be due both to the different texture and to the noise; then the objective is to separate the noise from the effect of texture variations.

In order to achieve this aim a small squared window n×n pixels (for e.g., 3×3 pixels) wide is moved within the area by a 3 pixel step and the DN mean (M_w) and the standard deviation (σ_w) is calculated for each window. The total DN range is divided in classes and the standard deviations are assigned to a class according to the mean DN of each window. At this stage, each class contains all the standard deviations attaining to those windows whose mean DN is within the DN limits of the class. It is reasonable that the lowest standard deviation are mainly due to the noise, whereas the other and for sure the highest are due to texture variations. Therefore in each class, the standard deviations are sorted, and the noise is estimated as the mean of the 5% smallest standard deviations. A check of the effectivenes of this hypothesis over a suitable simulated image is illustrated in [3].

2.2 Post-Flight Modulation Transfer Function (MTF) Analysis

The MTF of an imaging system describes the transfer of an input in spatial frequency domain. It is well known that MTF is a useful tool to describe the sharpness of an imaging system. Most of the time, the MTF characteristics are measured before the launch; however, they may change due to the vibration during the launch or some change in material properties in time. For that reason, for on-orbit MTF determination it is necessary to have an up-to-date performance assessment of spaceborne sensors.

Here it was evaluated according to the "Edge Method" proposed by Choi [2] and revisited by De Vendictis [5].

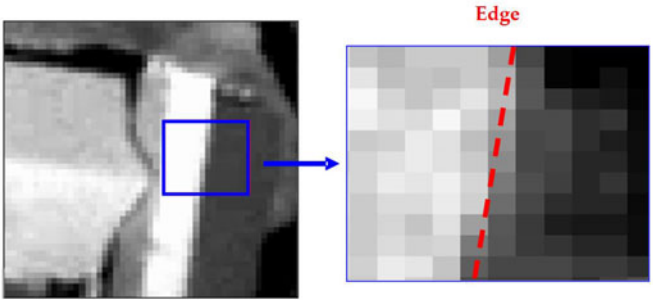

Fig. 1. Edge example

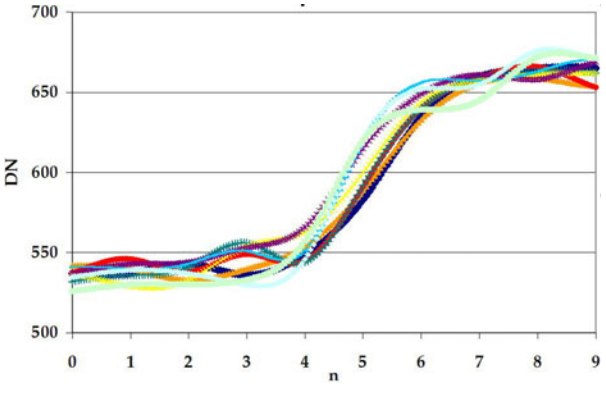

Fig. 2. Splines interpolating perpendicular lines

The initial task of the Edge Method is the identification of target edges useful for the analysis. Edges should show a blurred line edge between two almost uniform regions (at least in the neighborhood of the edge) of different intensities. Possible natural edges can be the separation line between the two layers of a roof, two fields with different cultivations, a roof edge and the ground, a road border and so on (Fig. 1).

After the selection of some suitable edges, at first the algorithm estimates the edge locations at sub-pixel accuracy; under the assumption that the chosen edges lie on a straight line, the alignment of all edge locations is LS estimated. The edge profiles, which are centered at each edge pixel and have the direction perpendicular to the edge, are interpolated with cubic spline functions (Fig. 2).

These cubic spline functions, differently from Choi, are averaged and interpolated with an analytical function in order to obtain an empirical Edge Spread Function (ESF) (Fig. 3).

The ESF is then differentiated to obtain the Line Spread Function (LSF). Finally the LSF is Fourier-transformed and normalized to obtain the corresponding

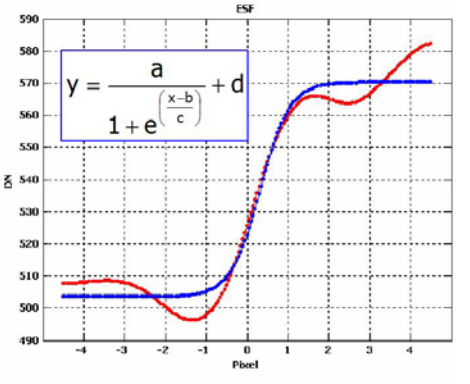

Fig. 3. Empirical Edge Spread Function in blue color

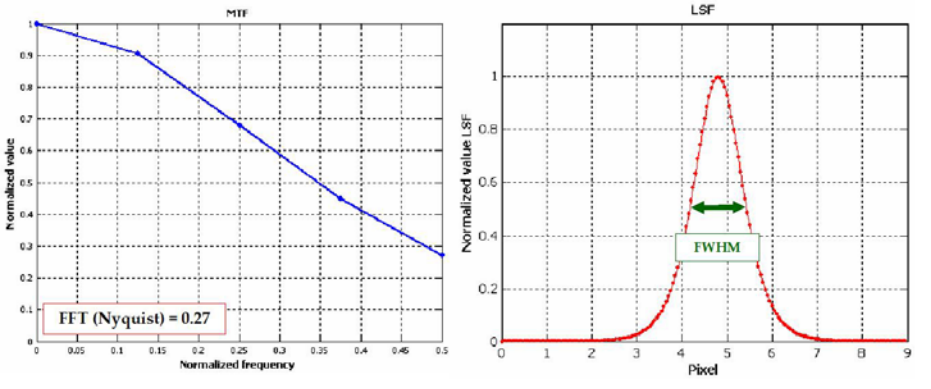

Fig. 4. MTF at Nyquist frequency and Full Width at Half Maximum

MTF. Finally, after the Fourier transformation, the computed MTF is scaled in the frequency axis in order to represent the calculated MTF in terms of the Nyquist frequency of the image. In addition, the Full Width at Half Maximum (FWHM) value is also computed from the estimated LSF (Fig. 4).

The details of both procedures are described exhaustively in [3].

3 Results of Radiometric Quality Analysis

Geoeye-1 imagery are collected in 11-bits format (2048 grey levels) but, even if the peak is less pronounced, the 99% of the DN vary between 110 and 780. For this reason, in order to perform the signal-to-noise ratio analysis, the imagery DN interval between 110 and 782, with the exclusion of the histogram tails (0-110 DN and 782-2047 DN), has been divided in different classes, 32 grey levels wide.

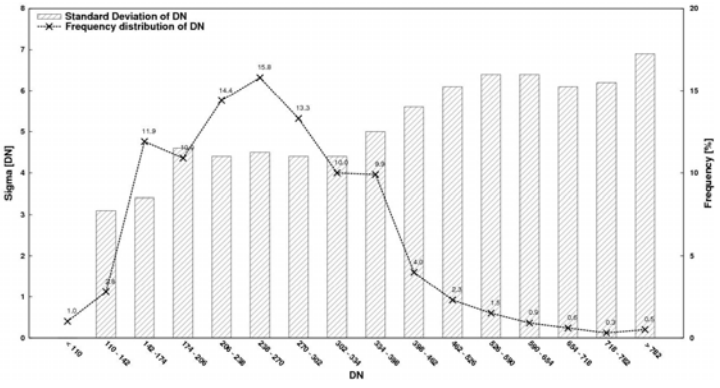

Fig. 5. Geoeye-1 noise level estimation

The analysis results are reported in Fig. 5 showing that the noise is intensity dependent, in fact it is increasing with increasing grey values.

The MTF was estimated detecting, on the whole image, 30 well distributed linear structures, oriented both along- and across-track. The MTF values at Nyquist frequency and the FWHM values were estimated for all the selected edges; the results were combined into average values for the along- and across-track direction (Tab. 1).

Table 1. MTF and FWHM estimation

Off Nadir	Sun elevation	Resampling	Edges along-track		Edges cross-track	
			MTF at Nyquist	FWHM (pixel)	MTF at Nyquist	FWHM (pixel)
12°	50°	CC	0.42	1.05	0.34	1.18

The results achieved show that the MTF values and the FWHM values seem to be similar for along and cross track direction, considering their standard deviation at the level of 0.15.

They seem to be slightly better than those displayed in [8], that states as reference for Geoeye-1 a MTF value at the Nyquist frequency of approximately 0.24 along-track and 0.26 across-track; due to the high MTF standard deviation this issue has to be investigated repeating the analysis on other images. Anyway it has to be noticed that tests discussed by Kohm were carried out on images acquired just 6 months after the launch, which could suffer for an initial non optimal radiometric calibration.

4 Orientation Models for High Resolution Satellite Imagery

Image distortions, due to acquisition system and geometry, could be removed by an orientation process, estimating a set of parameters for an orientation model. Remote sensing community usually adopts two different types of orientation models for High Resolution Satellite Imagery (HRSI): the physical sensor models (also called rigorous models) and the generalized sensor models.

The rigorous models are based on a standard photogrammetric approach where the image and the ground coordinates are linked through collinearity equations. The involved parameters have physical meaning. Besides, they require the knowledge of the specific satellite and orbit characteristics.

On the contrary, the generalized models are usually based on the RPFs which link image and terrain coordinates by the RPCs and do not need the knowledge of sensor and acquisition features. The RPCs can be calculated by the final users via a LS estimation directly from GCPs, or are generated by the sensor managing companies by using their own physical sensor models and disseminated to the users through the image metadata. Nevertheless, the first strategy (also called terrain-dependent) is not recommended if a reliable and accurate orientation is required. In the second strategy, they can be generated according to a terrain-independent scenario based on a known physical sensor model.

This section will discuss many features of the orientation models. Specifically, in Sect. 4.1 discussions will be focused on the rigorous model for the orientation of the image projected to a specific object surface (usually an "inflated" ellipsoid derived from the WGS84) (level 1B). The RPCs model is discussed in Sect. 4.2 and Sect. 4.3.

4.1 The Rigorous Model for Level 1B Imagery

This specific rigorous model has been developed for the management of level 1B imagery [4]. In this case it has to be noted that the images are projected onto a specific object (usually an "inflated" ellipsoid, derived from the WGS84 choosing a certain ellipsoidal height). The collinearity equations link points on the ground and points projected on the mentioned "inflated" ellipsoid (Fig. 6).

Each point on the ground surface corresponds to a point on "inflated" ellipsoid, identified from line of sight (LOS), i.e. the line directed from the perspective centre to the point on the ground. The collinearity condition is satisfied when $\hat{u}_{SI}$ (the unit vector directed from perspective centre to image point) coincides with $\hat{u}_{ST}$ (the unit vector directed from perspective centre to ground point), i.e., ground point and image point are lined up on LOS. The collinearity equations may be conveniently expressed in the ECEF system in vector form:

$$\hat{u}_{SI} = \mathbf{R} \cdot \hat{u}_{ST} \tag{1}$$

where $\mathbf{R}$ is a rotation matrix. In fact, relative "small" translation of ground with respect to ellipsoid can be expressed with an infinitesimal rotation around the

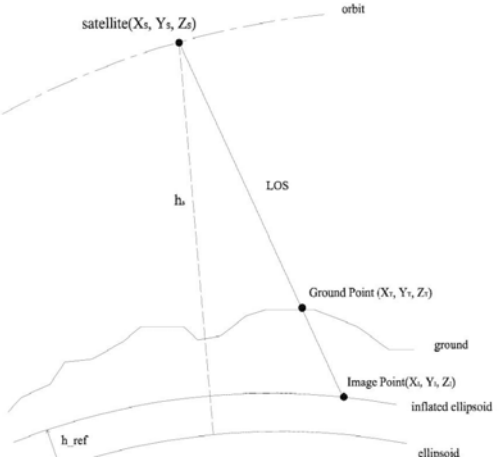

Fig. 6. Model geometry of level 1B image

perspective center, because the height of satellite platform (h_S) is much higher than the difference of elevation between ground surface and the "inflated" ellipsoid (Δh). Under this infinitesimal rotation hypothesis ($cos\phi, \theta, \psi \cong 1\ sin\phi \cong \phi, sin\theta \cong \theta, sin\psi \cong \psi$) the rotation matrix $\mathbf{R}$ is reduced to the sum of the unit matrix and an antisymmetric matrix:

$$R = I + \delta R = \begin{bmatrix} 0 & \varphi & \theta \\ -\varphi & 0 & \psi \\ -\theta & -\psi & 0 \end{bmatrix} \Rightarrow R = \begin{bmatrix} 1 & \varphi & \theta \\ -\varphi & 1 & \psi \\ -\theta & -\psi & 1 \end{bmatrix} \tag{2}$$

where the attitude angles are supposed to be modelled by a time-dependent function up to the second order (3).

$$\begin{cases} \varphi = a_0 + a_1\tau + a_2\tau^2 \\ \vartheta = b_0 + b_1\tau + b_2\tau^2 \\ \psi = c_0 + c_1\tau + c_2\tau^2 \end{cases} \tag{3}$$

τ is the time, in seconds, such as $\tau = J_s \cdot \Delta t$ where Δt is the time needed to scan a row on the ground and J_s is the row of the pixel.

The (1) can also be expressed in the following way:

$$\begin{bmatrix} X_I - X_S \\ Y_I - Y_S \\ Z_I - Z_S \end{bmatrix} = \rho R \begin{bmatrix} X_T - X_S \\ Y_T - Y_S \\ Z_T - Z_S \end{bmatrix} \tag{4}$$

where

- ϱ is the scale factor, (ratio of perspective centre-image point distance d_{SI} and perspective centre-ground point distance d_{ST}: $\rho = d_{SI}/d_{ST}$)
- X_T, Y_T, Z_T are the ground coordinates in the ECEF system

- X_I, Y_I, Z_I are the image coordinates in the ECEF system
- X_S, Y_S, Z_S are the perspective centre coordinates in the ECEF system

The model parameters that need to be estimated with the LS adjustment are the nine coefficients (a_i, b_i, c_i). Their initial approximate values are simply fixed to zero.

As regards the satellite position, in general detailed information are not supplied for the level 1B images; therefore the satellite coordinates can be roughly computed only on the basis of the angles (azimuth and elevation) that define satellite position with respect to image center. Nevertheless, this way is often rather inaccurate, so that it is necessary to follow an other strategy.

In particular in this work Direct Linear Transformation (DLT) is used, establishing a rough relation between image coordinates and ground coordinates in a Cartesian Local system.

The DLT is based on the following equations:

$$\begin{array}{l} I = \frac{L_1 \cdot E + L_2 \cdot N + L_3 \cdot U + L_4}{L_9 \cdot E + L_{10} \cdot N + L_{11} \cdot U + 1} \\ J = \frac{L_5 \cdot E + L_6 \cdot N + L_7 \cdot U + L_8}{L_9 \cdot E + L_{10} \cdot N + L_{11} \cdot U + 1} \end{array} \tag{5}$$

where (I, J) are the image coordinates, (E, N, U) are the ground coordinates respect to the Cartesian Local system centered in the center of the image and the L_i are the DLT parameters.

Starting from some GCPs coordinates, the DLT parameters are estimated; satellite position in the Cartesian Local system, related to the image center, is computed using the DLT parameters for a fixed height of the satellite.

Local coordinates are transformed into ECEF coordinates, and from the unique satellite position it is possible to reconstruct the orbit segment. Due to the short lenght of the orbital arc related to the image acquisition, it is possible to approximate it with an arc of circumference. Details on this computation, which is conveniently done in the orbital system, are illustrated in [4].

4.2 RPC Usage and Orientation Refinement in RPF

As mentioned before, some companies (for example DigitalGlobe for QuickBird and WorldView and Space Imaging for Ikonos and GeoEye-1, India Space Research Organization for Cartosat-1) usually supply the RPCs, as part of the image metadata to enable image orientation via RPFs.

The RPFs relate object point coordinates (latitude φ, longitude λ and height h) to pixel coordinates (I, J), as a physical sensor models, but in the form of ratios of polynomial expressions:

$$I = \frac{P_1(\varphi, \lambda, h)}{P_2(\varphi, \lambda, h)} \qquad J = \frac{P_3(\varphi, \lambda, h)}{P_4(\varphi, \lambda, h)} \tag{6}$$

where φ, λ are the geographic coordinates, h is the height above the WGS84 ellipsoid and (I, J) are the image coordinates. The order of these four polynomials is usually limited to 3 so that each polynomial takes the generic form:

$$P_n = \sum_{i=0}^{m_1} \sum_{j=0}^{m_2} \sum_{k=0}^{m_3} t_{ijk} \varphi^i \lambda^j h^k \tag{7}$$

with $0 \leq m_1 \leq 3$; $0 \leq m_2 \leq 3$; $0 \leq m_3 \leq 3$ and $m_1 + m_2 + m_3 \leq 3$, where t_{ijk} are the RPCs [9].

The ground and image coordinates $(\varphi, \lambda, h; I, J)$ in the equation (6) are normalized to (-1, +1) range using normalization parameters supplied in the metadata file, in order to improve the numerical precision during the computation.

Since the residual bias may be present into the RPCs, the orientation can be refined on the basis of the known GPs, acting as GCPs. A possible refinement of the model (6) (written in normalized coordinates), allowing for bias compensation, is accomplished in a quite common way with the introduction of a simple first order polynomial in the RPFs (8) whose parameters are estimated, provided a suitable number of GCPs is known [7].

$$\begin{aligned}
&I_n = A_o + I_n \cdot A_1 + J_n \cdot A_2 + \tfrac{P_1(\varphi_n, \lambda_n, h_n)}{P_2(\varphi_n, \lambda_n, h_n)} = \\
&= A_o + I_n \cdot A_1 + J_n \cdot A_2 + \tfrac{a_0 + a_1\lambda_n + a_2\varphi_n + a_3 h_n + a_4\lambda_n\varphi_n + \ldots + a_{17}\lambda_n^3 + a_{18}\varphi_n^3 + a_{19}h_n^3}{1 + b_1\lambda_n + b_2\varphi_n + b_3 h_n + b_4\lambda_n\varphi_n + \ldots + b_{17}\lambda_n^3 + b_{18}\varphi_n^3 + b_{19}h_n^3} \\
&J_n = B_o + J_n \cdot B_1 + I_n \cdot B_2 + \tfrac{P_3(\varphi_n, \lambda_n, h_n)}{P_4(\varphi_n, \lambda_n, h_n)} = \\
&= B_o + J_n \cdot B_1 + I_n \cdot B_2 + \tfrac{c_0 + c_1\lambda_n + c_2\varphi_n + c_3 h_n + c_4\lambda_n\varphi_n + \ldots + c_{17}\lambda_n^3 + c_{18}\varphi_n^3 + c_{19}h_n^3}{1 + d_1\lambda_n + d_2\varphi_n + d_3 h_n + d_4\lambda_n\varphi_n + \ldots + d_{17}\lambda_n^3 + d_{18}\varphi_n^3 + d_{19}h_n^3}
\end{aligned} \tag{8}$$

where (I_n, J_n) are the normalized images coordinates, and P_i are third order polynomial functions of object space normalized coordinates $(\varphi_n, \lambda_n, h_n)$; A_i and B_i terms describe image shift and drift effects in particular:

- $A_0, A_1, A_2, B_0, B_1, B_2$ describe a complete affine transformation
- A_0, A_1, B_0, B_1 model the shift and drift
- A_0, B_0, describe a simple coordinate shift

4.3 RPC Generation by SISAR Rigorous Model

In this Section will be discuss the strategy for the RPCs generation using the already established physical sensor model.

A 2D image grid covering the full extent of the image is established and its corresponding 3D object grid with several layers (e.g., four or more layers for the third-order case) slicing the entire elevation range is generated. The horizontal coordinates (X, Y) of a point of the 3D object grid are calculated from a point (I, J) of the image grid using the physical sensor model with an a priori selected elevation Z. Then, the RPC are LS estimated with the object grid points and the image grid points. This terrain-independent computational scenario can make the RPFs model a good replacement to the physical sensor models, and has been widely used to determine the RPCs.

It has to be underlined that in the usually adopted terrain-independent approach, the LS solution is often carried out through a regularization, since unknown RPCs may be highly correlated so that the design matrix is almost rank deficient. In order to overcome the regularization requirements, an innovative

algorithm for the RPCs extraction, with a terrain independent approach, has been proposed in [4] and is shortly summarized hereafter.

In details, at first an image discretization is made, dividing the full extent image space in a 2D grid. Then, the points of the 2D image grid are used to generate the 3D ground grid: the image is oriented and by the knowledge of the rigorous orientation sensor model, the collinearity equations were derived and used to create the 3D grid, starting from each point of the 2D grid image. In this respect, it has to be noted that the 2D grid is actually a regular grid, whereas the 3D one is not strictly regular, due to the image attitude. Moreover, the 3D grid points were generated intersecting the straight lines modelled by the collinearity equations with surfaces (approximately ellipsoids) concentric to the WGS84 ellipsoid, placed at regular elevation steps. So, the dimension of the 3D grid is both based on the full extent of the image and the elevation range of the terrain (Fig.7).

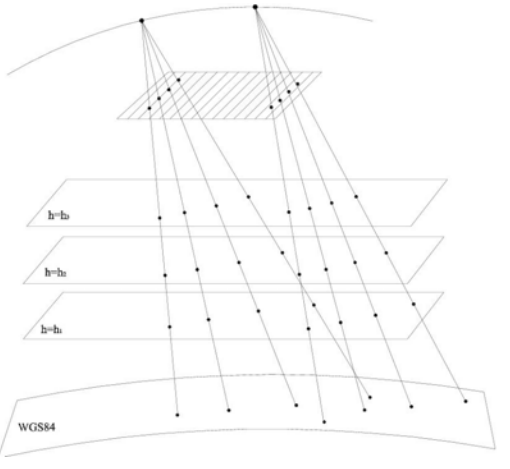

Fig. 7. Grid for RPC generation in the terrian-independet approach

The RPCs least squares estimation is based on the linearization of the generic RPFs equations, which can be written as:

$$\begin{aligned} &I_n + b_1\lambda_n I_n + b_2\varphi_n I_n + ... + b_{19}h_n^3 I_n - a_0 - a_1\lambda_n - a_2\varphi_n ... - a_{19}h_n^3 = 0 \\ &J_n + d_1\lambda_n J_n + d_2\varphi_n J_n + ... + d_{19}h_n^3 J_n - c_0 - c_1\lambda_n - c_2\varphi_n ... - c_{19}h_n^3 = 0 \end{aligned} \tag{9}$$

where a_i, b_i, c_i, d_i are the RPCs (78 coefficients for third order polynomials), (I_n, J_n) and $(\varphi_n, \lambda_n, h_n)$ are the normalized coordinates, with scale and offset factors computed according to:

$$\begin{cases} w_{offset} = \min(w_k) \\ w_{scale} = \max(w_k) - \min(w_k) \end{cases} where\ w = \varphi, \lambda, h$$
$$\begin{cases} I_{offset} = J_{offset} = 1 \\ I_{scale} = n^\circ column - 1 \\ J_{scale} = n^\circ row - 1 \end{cases} \tag{10}$$

where k is the number of available GCPs and n° column/row are the overall columns/rows of the image; the normalization range is (0, 1).

The new proposed estimation approach is based on the Singular Value Decomposition (SVD) and QR decomposition which are employed to evaluate the actual rank of the design matrix and to select the actual estimable coefficients; again, the SVD based subset selection procedure is due to Golub, Klema and Stewart [6]. This method permits to select only the really estimable and significant parameters, avoiding an over-parametrization; so, the number of estimated coefficients is usually less than the vendors one (about 1/2 ,1/3 coefficients).

5 Results of Geometric Analysis of GeoEye-1 Image

This Section is focused on the evaluation of the geometric capability of Geoeye-1 satellite. The data analysed is a GeoEye-1 image, that has been oriented using two different methods: the rigorous model and the RPFs model with the RPCs.

Orientation has been performed with two different software:

- the commercial software PCI Geomatica 10.2, in which is embedded the OrthoEngine module, equipped with the rigorous model developed by Toutin [10]
- the scientific software SISAR developed by the Geodesy and Geomatic Area of "La Sapienza" University of Rome, in which the rigorous model and a routine for RPC generation are included

The results were analysed in order to compare the orientation quality obtained from different models and different software in terms of accuracy achievable from the image.

In the Tab. 2 the features of the GeoEye-1 image are listed. The panchromatic analysed image was acquired on 21 September 2009, it has 0.5 m pixel size and belongs to the Geo product class.

The GPs were surveyed with static or fast static procedures by a Trimble 5700 GPS receiver and their coordinates are estimated by Trimble Geomatic Office software with respect to available GPS permanent stations (M0SE at Rome Faculty of Engineering). The mean horizontal and vertical accuracies of the coordinates are between 10 and 20 cm.

The entire scene is split into two tiles, and each of them is provided with a specific vendors RPC file. In the case of orientation with rigorous model it possible to stitch two tiles and to handle the entire scene. On the other hand, in the case of RPCs model the two tiles have to be oriented separately, because they have two different RPCs files.

Thanks to the SISAR routine for the RPCs generation, a unique RPCs file can be obtained, suitable to orientate the entire scene with RPCs model; moreover the SISAR RPCs can be easily loaded into any commercial software.

5.1 Rigorous Model Results

The image has been oriented with rigorous models implemented in SISAR and in OrthoEngine. The orientation tests have been performed varying the number

Table 2. Features of GeoEye-1 image

Area	GSD [m]	Off-nadir [°]	Scene coverage [Km x Km]	GPs
Rome	0.50	12	16 × 15	37

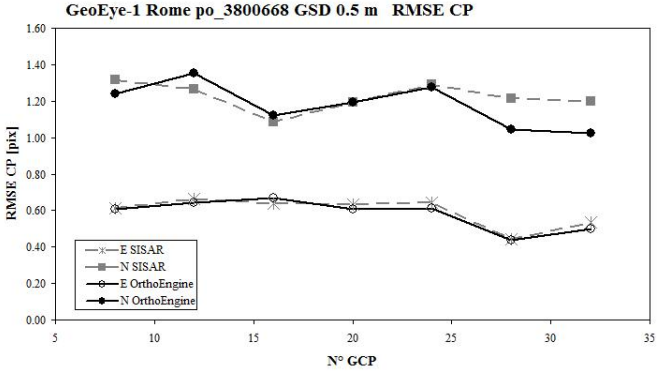

Fig. 8. Rigorous model - Image accuracy vs. GCP number for GeoEye-1 image of Rome

of GCPs and the image accuracy, represented by the RMSE computed over Check Points (CPs) residuals (CPs RMSE), was been analyzed. The RMSEs were computed both for the North and East residual components separately.

RMSE trend is similar for both software and accuracy value is around the GSD value; in particular CPs RMSE is approximately 0.30 m in East component and 0.60 m North component.

5.2 RPCs Vendors Results

As mentioned, the Rome GeoEye-1 scene is composed by two tiles, that are provided with two different RPCs files; therefore the two tiles have been oriented separately, which could be a remarkable drawback for several applications. In Tab. 3 the results, obtained using the vendors RPCs, are listed respectively for the first and the second tile of the Rome scene. Accuracy in terms of CPs RMSE has been evaluated for the RCPs orientation performed without adjustment, estimating both shift and affine trasformation using 5 GCPs.

Note that the results are quite different for the two tiles; moreover, the accuracy for the East component is always in the order of one pixel, whereas for the North component the shift and affine transformation improve the results significantly; it has to be underlined that the shift transformation performs slighly better and seems to be enough to model the correction, as already proven with other level 1B imagery (for example Ikonos ones).

Table 3. Results of GeoEye-1 image orientation with vendors RPCs

RMSE CP [pix]						
OrthoEngine						
	First Tile			**Second Tile**		
	n° GCP	EAST	NORTH	n° GCP	EAST	NORTH
Without correction	-	0.91	8.41	-	1.06	8.29
Shift transformation	5	0.68	1.02	5	1.07	2.08
Affine transformation	5	0.87	1.07	5	1.13	2.13
SISAR						
	First Tile			**Second Tile**		
	n° GCP	EAST	NORTH	n° GCP	EAST	NORTH
Without correction	-	1.24	7.66	-	0.74	2.79
Shift transformation	5	0.66	0.90	5	1.03	1.78
Affine transformation	5	0.93	0.87	5	1.10	1.54

5.3 SISAR RPCs Results

In Fig. 9 and in Fig. 10 results of SISAR RPCs application are shown. The RPCs file has been obtained by a routine implemented in the software SISAR, that computes the coefficients on the basis of the rigorous model. A unique file, with 20 significant coefficients only, has been generated in order to orientate the entire scene.

SISAR RPCs are tested in the scientific SISAR software and in the commercial software OrthoEngine. It has to be noticed that the results are totally comparable with the rigorous ones, and the CPs RMSE trend is quite similar for the two software. Moreover, the results obtained using a shift and an affine transformation are respectively presented; again, the affine model does not improve significantly the accuracy achivable with the RPCs.

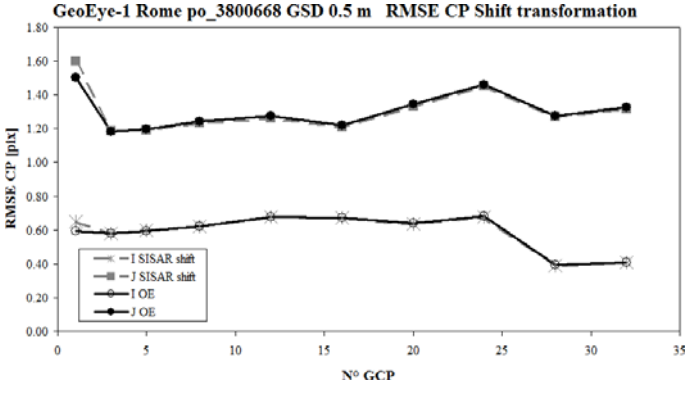

Fig. 9. SISAR RPCs, shift transformation - Image accuracy vs. GCP number for GeoEye-1 image of Rome

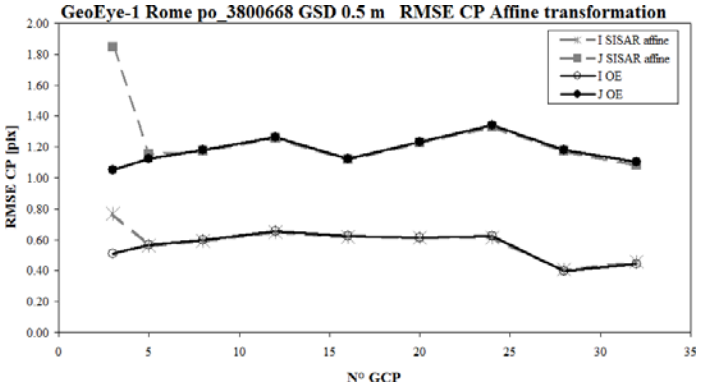

Fig. 10. SISAR RPCs, affine transformation - Image accuracy vs. GCP number for GeoEye-1 image of Rome

6 Conclusions

The GeoEye-1 satellite is able to acquire panchromatic and multispectral images at very high resolution. The paper presents an analysis about the radiometric and geometric features of a very recent image acquired on September 2009 over Rome (Italy).

As regard to the radiometric analysis, the results show that the noise is intensity dependent, in fact it is increasing with increasing grey values.

The MTF values at Nyquist frequency and the FWHM values were estimated for all the selected edges; the results were combined into average values for the along- and across-track direction. The results achieved show that the MTF values and the FWHM values seem to be similar for along and cross track direction, considering their standard deviation at the level of 0.15.

As regard to the geometric capability, the accuracy of the orientation performed with two software (PCI OrthoEngine and SISAR) is on the order of the pixel size, both using rigorous model and RPCs model, almost twice better in East than in North component.

In particular, the autonomously generated SISAR RPCs, which overcome the problem of the vendors RPCs related to two separated tiles, can be used also by commercial software (like OrthoEngine); commercial software results using SISAR RPC are comparable with the results obtained using vendors RPC in the same software and globally even better.

Moreover it possible to note that the simple shift adjustment eliminates almost the totality of RPC geolocation errors, as already encountered with level 1B imagery.

References

1. Baltsavias, E.P., Pateraki, M., Zhang, L.: Radiometric and Geometric Evaluation of IKONOS Geo Images and Their Use for 3D Building Modeling. In: Joint ISPRS Workshop on High Resolution Mapping from Space (2001)
2. Choi, T.: IKONOS Satellite on Orbit Modulation Transfer Function (MTF) Measurement using Edge and Pulse Method. Master Thesis, South Dakota State University (2002)
3. Crespi, M., De Vendictis, L.: A Procedure for High Resolution Satellite Imagery Quality Assessment. Sensors 9(5), 3289–3313 (2009)
4. Crespi, M., Fratarcangeli, F., Giannone, F., Pieralice, F.: Chapter 4 - Overview on models for high resolution satellites imagery orientation. In: Li, D., Shan, J., Gong, J. (eds.) Geospatial Technology for Earth Observation data. Springer, Heidelberg (2009)
5. De Vendictis, L.: Quality assessment and enhancement of High Resolution Satellite Imagery for DSM extraction. PhD Thesis, Area di Geodesia e Geomatica Dipartimento di Idraulica Trasporti e Strade, Sapienza Universit di Roma (2007)
6. Golub, G.H., Van Loan, C.F.: Matrix Computation. The Johns Hopkins University Press, Baltimore and London (1993)
7. Hanley, H.B., Fraser, C.S.: Sensor orientation for high-resolution satellite imagery: further insights into bias-compensated RPC, `http://www.isprs.org/istanbul2004/comm1/papers/5.pdf`
8. Kohm, K., Mulawa, D.: On-Orbit Geolocation Accuracy andImage Quality Performance of the GeoEye-1High Resolution Imaging Satellite. In: GeoEye JACIE Conference Fairfax, Virginia (2009)
9. Tao, C.V., Hu, Y.: 3D reconstruction methods based on the rational function model. Photogrammetric Engineering & Remote Sensing 68(7), 705–714 (2002)
10. Toutin, T.: Geometric processing of remote sensing images: models, algorithms and methods (review paper). International Journal of Remote Sensing 10, 1893–1924 (2004)
11. Zhang, L.: Automatic Digital Surface Model (DSM) Generation from Linear Array Images. PhD Dissertation, Institute of Geodesy and Photogrammetry, ETH Zurich (2005), ISBN 3-906467-55-4